Distorted-wave calculations of the electron-impact ionization of highly ionized Na-like ions

D. C. Griffin*
Joint Institute for Laboratory Astrophysics, University of Colorado and National Bureau of Standards, Boulder, Colorado 80309

M. S. Pindzola
Department of Physics, Auburn University, Auburn, Alabama 36849

C. Bottcher†
Physics Division, Argonne National Laboratory, Argonne, Illinois 60439
(Received 7 May 1987)

We report on distorted-wave calculations of the electron-impact ionization cross sections and rate coefficients for the Na-like ions Ti^{11+}, Cr^{13+}, Fe^{15+}, and Ni^{17+}. The cross sections for direct ionization out of the $3s$, $2p$, and $2s$ subshells were determined using the configuration-average, distorted-wave approximation. In addition, excitation-autoionization contributions originating from inner-shell excitations of the type $2s^22p^63s \rightarrow 2s^22p^53snl$ ($n=3,4,5$) and $2s^22p^63s \rightarrow 2s2p^63snl$ ($n=3,4$) were calculated by employing the distorted-wave approximation and configuration-interaction, bound-state wave functions. Near threshold, the total-ionization cross sections in all four ions are enhanced by approximately a factor of 5 through excitation autoionization. These excitation-autoionization contributions are large, even though they have been substantially reduced by radiative decay to the bound states of the initial ion. Furthermore, although electron correlation has a minimal effect on the excitation cross sections, the magnitude of the branching ratios for autoionization is quite sensitive to configuration interaction in the autoionizing levels. This is especially true for the $2p \rightarrow 3d$ excitations, where configuration interaction between $2p^53s3d$ and $2p^53p^2$ can increase the magnitude of the autoionizing rates for levels within the $2p^53s3d$ configuration by as much as three orders of magnitude. Thus, for example, in the case of the $2p \rightarrow 3d$ excitation in Ni^{17+}, correlation increases the overall branching ratio for autoionization from 0.27 to 0.53.

I. INTRODUCTION

A number of collisional processes can contribute to the total electron-impact ionization of Na-like ions. In addition to direct ionization from an initial ion with atomic number Z and $N=11$ bound electrons

$$e^- + X(Z,N) \rightarrow X(Z,N-1) + e^- + e^- , \quad (1)$$

we have inner-shell excitation followed by autoionization

$$e^- + X(Z,N) \rightarrow X^{**}(Z,N) + e^- \quad (2)$$
$$\searrow\ X^{*}(Z,N-1) + e^-$$

and resonant recombination to the Mg-like ion followed by double autoionization

$$e^- + X(Z,N) \rightarrow X^{**}(Z,N+1)$$
$$\searrow\ X^{**}(Z,N) + e^-$$
$$\searrow\ X^{*}(Z,N-1) + e^- . \quad (3)$$

The effects of indirect processes on the electron-impact ionization of Na-like ions have been studied extensively. Bely[1,2] employed Coulomb-Born results scaled from Fe^{16+} to estimate excitation-autoionization contributions to the ionization of Mg^+, Al^{2+}, P^{4+}, Ca^{9+}, and Fe^{15+}, and Moores and Nussbaumer[3] employed the Coulomb-Born approximation to determine the effects of excitation autoionization on the ionization cross section for Mg^+. Cowan and Mann[4] employed distorted-wave calculations of the inner-shell excitations and intermediate-coupled, single-configuration calculations of the branching ratios for autoionization to determine the contributions of excitation autoionization to the total ionization rate coefficient for Fe^{15+}, and thereby demonstrated the importance of radiative relaxation in highly ionized systems. LaGuttata and Hahn[5] employed a configuration-average, distorted-wave approximation and average branching ratios to calculate the excitation-autoionization contributions as well as the contributions of resonant recombination followed by double autoionization to the ionization cross section of Fe^{15+}.

Martin *et al.*[6] made the first crossed electron-ion beam measurements of the ionization cross section of Mg^+; however, they were not able to detect any abrupt increases in the cross section due to excitation autoionization and estimated that such effects should be less than 7% in this ion. More recent crossed-beam measurements by Crandall *et al.*[7] for Mg^+, Al^{2+}, and Si^{3+} reveal that excitation-autoionization contributions are at the 15% level near threshold in Mg^+, at the 30% level near threshold in Al^{2+}, and that they more than double the total-ionization cross section near threshold in Si^{3+}. Distorted-wave calculations of the excitation-

autoionization contributions for these three ions[8] are larger than the experimentally determined indirect effects by nearly a factor of 2; close-coupling calculations[9] are in better agreement with experiment, but still overestimate the magnitude of the $2p \rightarrow 3p$ excitation, which provides the largest indirect contribution in these low stages of ionization.

Recently, Gregory *et al.*[10] measured the cross section of Fe^{15+}, and their measurements indicate that indirect processes increase the total-ionization cross section by more than a factor of 5 near threshold. These measurements appear to be in reasonably good agreement with the calculations of the excitation-autoionization contributions of LaGattuta and Hahn,[5] but do not show evidence of the large contributions due to resonant recombination followed by double autoionization that were predicted in Ref. 5.

In this paper we report on extensive calculations of the total-ionization cross sections of the highly ionized Na-like ions Ti^{11+}, Cr^{13+}, Fe^{15+}, and Ni^{17+}. All of these ions are important impurities in laboratory plasmas, and accurate ionization rate coefficients are required for the modeling of such plasmas. Furthermore, for these ions, the effects of coupling between scattering channels are expected to be sufficiently small that the distorted-wave approximation should be quite accurate; however, a systematic study of coupling as a function of ionization stage is needed to confirm this point. Finally, radiative decay rates are comparable in magnitude to the autoionizing rates in all of these ions, and the effects of configuration interaction on the branching ratio for autoionization can be quite important.

The remainder of this paper is arranged as follows. In Sec. II we describe the theoretical and calculational methods employed to determine the ionization cross sections and rate coefficients. In Sec. III we first describe, in detail, the results of our calculations of the excitation-autoionization contributions in Ni^{17+}. We then present the theoretical ionization cross sections and rate coefficients for all four ions, and compare our near-threshold cross sections for Fe^{15+} with the experimental measurements and other calculations. Finally in Sec. IV we summarize our results and consider their implications.

II. THEORETICAL AND CALCULATIONAL METHODS

If we ignore the contributions of resonant recombination followed by double autoionization and assume that direct ionization and excitation autoionization are independent processes, then the total-ionization cross section is given by

$$\sigma_{\rm tot}(i)=\sum_f \sigma_{\rm ion}(i\rightarrow f)+\sum_j \sigma_{\rm exc}(i\rightarrow j)B_j^a \ , \tag{4}$$

where $\sigma_{\rm ion}(i\rightarrow f)$ is the average ionization cross section from the initial configuration i to the final configuration f of the $(N-1)$-electron ion; $\sigma_{\rm exc}(i\rightarrow j)$ is the inner-shell excitation cross section from the initial configuration i to a particular autoionizing level j. B_j^a is the branching ratio for autoionization from the level j and is given by

$$B_j^a=\frac{\sum_m A_a(j\rightarrow m)}{\sum_m A_a(j\rightarrow m)+\sum_k A_r(j\rightarrow k)} \ , \tag{5}$$

where $A_a(j\rightarrow m)$ is the autoionizing rate from level j to the continuum channel m, and $A_r(j\rightarrow k)$ is the radiative rate from level j to a final bound level k.

The direct-ionization cross section is calculated in the configuration-average, distorted-wave approximation. For ionization of an electron within the subshell $n_b l_b$ with the occupation number q_b

$$e^- + (n_b l_b)^{q_b} \rightarrow (n_b l_b)^{q_b-1} + e^- + e^- \ , \tag{6}$$

the configuration-average ionization cross section is given by

$$\begin{aligned}\sigma_{\rm ion}(i\rightarrow f) &= \int_0^{E/2} dE_e \left[\frac{32 q_b}{k_i^3 k_e k_f} \sum_{l_i l_e l_f} (2l_i+1)(2l_e+1)(2l_f+1) \right. \\ &\times \left[\sum_\lambda A(l_e,l_f,l_b,l_i,\lambda)[R^\lambda(k_e l_e,k_f l_f;n_b l_b,k_i l_i)]^2 \right. \\ &+ \sum_{\lambda'} B(l_f,l_e,l_b,l_i,\lambda')[R^{\lambda'}(k_f l_f,k_e l_e;n_b l_b,k_i l_i)]^2 \\ &\left. \left. - \sum_\lambda \sum_{\lambda'} | C(l_e,l_f,l_b,l_i,\lambda,\lambda')R^\lambda(k_e l_e,k_f l_f;n_b l_b,k_i l_i)R^{\lambda'}(k_f l_f,k_e l_e;n_b l_b,k_i l_i) | \right] \right] .\end{aligned} \tag{7}$$

In this expression, we use atomic units; the continuum normalization is one times a sine function; we employ the maximum-interference approximation of Peterkop;[11] k_i, k_e, and k_f are the linear momenta of the incident, ejected, and scattered electrons, respectively; l_i, l_e, and l_f are the angular momenta of the partial waves for the incident, ejected, and scattered electrons, respectively; R^λ represents the usual Slater integrals; $E=(\frac{1}{2})k_i^2-I$, where I is the ionization potential; and E_e is the ejected electron energy $(=k_e^2/2)$. The angular coefficients of

the direct, exchange, and cross terms are given in terms of the 3-j and 6-j symbols by

$$A(l_e,l_f,l_b,l_i,\lambda)=\begin{pmatrix} l_e & \lambda & l_b \\ 0 & 0 & 0 \end{pmatrix}^2 \begin{pmatrix} l_f & \lambda & l_i \\ 0 & 0 & 0 \end{pmatrix}^2 \times(2\lambda+1)^{-1} , \quad (8)$$

$$B(l_f,l_e,l_b,l_i,\lambda')=\begin{pmatrix} l_f & \lambda' & l_b \\ 0 & 0 & 0 \end{pmatrix}^2 \begin{pmatrix} l_e & \lambda' & l_i \\ 0 & 0 & 0 \end{pmatrix}^2 \times(2\lambda'+1)^{-1} , \quad (9)$$

and

$$C(l_e,l_f,l_f,l_i,\lambda,\lambda') = [(2\lambda+1)(2\lambda'+1)A(l_e,l_f,l_b,l_i,\lambda) \times B(l_f,l_e,l_b,l_i,\lambda')]^{1/2} \begin{Bmatrix} l_e & l_b & \lambda \\ l_f & l_i & \lambda' \end{Bmatrix} . \quad (10)$$

In this work, the radial wave functions for the bound-state orbitals were calculated using the Hartree-Fock method with relativistic modifications (HFR),[12] which includes the mass-velocity and Darwin relativistic corrections within modified differential equations. The distorted-wave continuum orbitals were calculated using a local semiclassical approximation[13] for the exchange interaction.

Younger[14] has performed distorted-wave calculations of the direct-ionization cross section for the Na-like ions Mg^+, Al^{2+}, P^{4+}, and Ar^{6+} and fit these results to an extrapolation formula as a function of ionization state. We have performed calculations of the direct-ionization cross sections out of the $3s$, $2p$, and $2s$ subshell for Ni^{17+}, and have found that our cross sections are within 3% of those determined from Younger's formula. Therefore, his formula was employed to determine the direct-ionization cross sections for Ti^{11+}, Cr^{13+}, and Fe^{15+}.

In order to calculate direct-ionization cross sections at high energies, the formula of Younger[14]

$$\sigma_{\rm ion}=\frac{1}{IE_i}\left[A(1-1/u)+B(1-1/u)^2 +C\ln(u)+D\frac{1}{u}\ln(u) \right] \quad (11)$$

was employed, where E_i is the electron energy ($=k_i^2/2$) and $u=E_i/I$. The coefficients A, B, and D are determined from a least-squares fit to the calculated distorted-wave cross section, while C is a Bethe coefficient, determined from the photoionization cross section.[14]

In the distorted-wave approximation, the electron-impact excitation cross section from an initial level $\alpha_i J_i$ to a final level $\alpha_f J_f$ is given by

$$\sigma_{\rm exc}(i\rightarrow f)=\frac{4\pi}{k_i^3 k_f}\frac{1}{2(2J_i+1)}\sum_{l_i,l_f,j_i,j_f,J}(2J+1)\,|\,T(\alpha_f J_f l_f j_f J;\alpha_i J_i l_i j_i J)\,|^2 , \quad (12)$$

where J_i and J_f are the total angular momenta for the initial and final levels, respectively; α_i and α_f represent all other quantum numbers needed to specify the multiconfiguration, intermediate-coupled, initial and final levels, respectively; k_i and k_f are linear momenta of the incident and scattered electrons, respectively; l_i and l_f are the angular momenta of partial waves for the incident and scattered electrons, respectively; j_i and j_f are the total angular momenta of the partial waves for the incident and scattered electrons, respectively; and J is the total angular momentum of the $(N+1)$-electron system.

The T matrix for a given J and parity is related to the K matrix by the expression

$$T=-2iK(1-iK)^{-1} , \quad (13)$$

where

$$K_{fi}=-\langle \alpha_f J_f;l_f j_f J\,|\,H-E\,|\,\alpha_i J_i;l_i j_i J\rangle . \quad (14)$$

In order to calculate (14), we begin with the K matrix in a pure LS-coupling basis

$$K_{fi}(LS)=-\langle \beta_f L_f S_f;l_f LSJ\,|\,H-E\,|\,\beta_i L_i S_i;l_i LSJ\rangle . \quad (15)$$

We then transform the K matrix to a Jj-coupling basis

$$K_{fi}(Jj)=-\langle \beta_f L_f S_f J_f;l_f j_f J\,|\,H-E\,|\,\beta_i L_i S_i J_i;l_i j_i J\rangle . \quad (16)$$

Finally using intermediate-coupled, configuration-interaction eigenvectors calculated with the atomic structure program of Cowan[15]

$$|\,\alpha J\rangle=\sum_{\beta,L,S}Y^{\alpha J}_{\beta LS}\,|\,\beta LSJ\rangle , \quad (17)$$

we determine the K matrix in intermediate coupling. The continuum and bound-state orbitals used in the excitation calculations are identical to those described above for the determination of the direct-ionization cross sections.

For the results reported here, cross sections for individual inner-shell excitation transitions to each autoionizing level were calculated for energies just above the excitation threshold to approximately twice threshold with partial waves from $l=0$ to $l=12$. All individual cross sections were then extrapolated to an energy equal to twice the threshold energy of the most energetic inner-shell excitation included in the calculation.

In order to extend the calculations to still higher elec-

tron energies, and avoid making individual fits and extrapolations on the many hundreds of levels included in these calculations, the following procedure was used. We employed the configuration-average, distorted-wave approximation described in detail elsewhere[16] to determine the total excitation cross sections from the initial configuration to all final autoionizing configurations included in the detailed calculations, for partial waves from $l=0$ to $l=20$ and energies from just above the excitation threshold to four times threshold. These cross sections were then fit to a formula of the type

$$\sigma_{\rm exc}=\frac{1}{E_i}[A+B/u+C/u^2+D\ln(u)]\ , \tag{18}$$

where E_i is the electron energy of the initial electron and u is the electron energy divided by the threshold energy. For non-dipole-allowed transitions, D is equal to zero. The total excitation cross section for all inner-shell transitions calculated using (18) was then matched to the total excitation-autoionization cross section, including branching, from the detailed level-to-level calculations, and used to extrapolate the detailed calculations to higher energies. Since the cross sections to individual levels vary differently as a function of electron energy and the individual levels have different branching ratios for autoionization, the overall branching ratio for all excitation-autoionization contributions will be a function of energy, and this extrapolation procedure will not incorporate such a variation. However, our calculations indicate that this effect is small enough that the errors, which are only introduced at energies above twice the threshold energy of the most energetic inner-shell excitation, are less than 10%.

For modeling studies of impurities, ionization rate coefficients, rather than cross sections, are needed. The rate coefficient is defined as

$$\alpha=\int_0^\infty vf(v)\sigma(v)dv\ , \tag{19}$$

where $f(v)$ is the velocity distribution of electrons and $\sigma(v)$ is the total electron-impact ionization cross section as a function of electron velocity. If we assume a Maxwell-Boltzmann distribution of velocities, then, in units of $\rm cm^3/s$, the rate coefficient as a function of electron temperature is given by

$$\alpha(kT)=6.6924\times10^{-11}\frac{1}{(kT)^{3/2}}\int_0^\infty e^{-E/kT}\sigma(E)EdE\ , \tag{20}$$

where the electron energy E and the electron temperature kT are in eV, and the cross section is in units of 10^{-18} $\rm cm^2$. We have calculated the rate coefficients both by direct numerical integration and by integration of the cross-section fits in terms of known functions.

Finally, the natural logarithms of the rate coefficients can be fitted to a Chebyshev polynomial expansion following the method of Cox and Hayes.[17] One can then obtain the rate coefficients from any temperature kT from $E_{\rm min}$ to $E_{\rm max}$ using the equation

$$\alpha(kT)=\exp\left[a_0/2+\sum_{r=1}^{8}a_rT_r(x)\right]\ , \tag{21}$$

where α is again in units of $\rm cm^3/s$, $T_r(x)$ are the Chebyschev polynomials of the first kind,[18] a_r $(r=0,1,\ldots,8)$ are the fitting coefficients, and x is defined by the equation

$$x=\ln\left[\frac{(kT)^2}{E_{\rm min}E_{\rm max}}\right]\Big/\ln\left[\frac{E_{\rm max}}{E_{\rm min}}\right]\ , \tag{22}$$

with kT, $E_{\rm min}$, and $E_{\rm max}$ in units of eV. A fast method of evaluating Chebyshev polynomials has been developed by Clenshaw,[19] and a sample program which employs this method is given in Ref. 20.

III. RESULTS FOR THE Na-LIKE IONS

A. Excitation-autoionization contributions for Ni^{17+}

In the energy-level diagram of Fig. 1, we show the positions of the autoionizing configurations $2p^53snl$ $(n=3,4,5)$ and $2s2p^63snl$ $(n=3,4)$ for Ni^{17+} relative to the $2p^63s$ ground state and the configurations of Ni^{18+} produced by direct ionization out of the $3s$, $2p$, and $2s$ subshells. As can be seen, the only energetically possible autoionizing transitions are to the $2p^6$ ground state of Ni^{18+}.

We first consider the $2p^63s\rightarrow2p^53s^2$ and $2p^63s\rightarrow2p^53s3d$ transitions; the latter of these accounts for the largest indirect contribution to the total-ionization cross section. The configuration-interaction, distorted-wave calculation of the excitation cross section

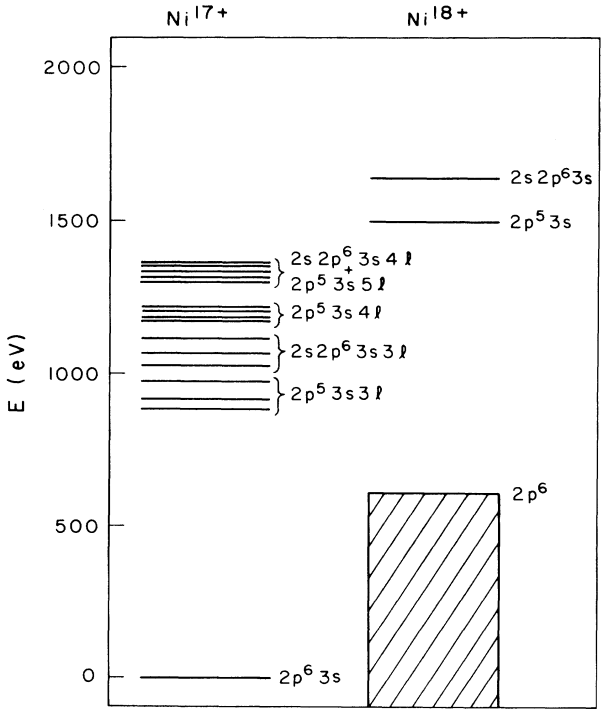

FIG. 1. Energy-level diagram showing the $2p^53snl$ and $2s2p^63snl$ autoionizing configurations of Ni^{17+} relative to the ionization thresholds for ionization from the $3s$, $2p$, and $2s$ subshells.

TABLE I. Excitation energies, radiative rates, autoionizing rates, and autoionizing branching ratios for Ni^{17+} calculated in a single-configuration approximation and with configuration interaction.

	Single configuration				Configuration interaction[a] ($2p^5 3s 3d + 2p^5 3s^2 + 2p^5 3p^2 + 2p^5 3d^2$)			
J	E (eV)	A_r (10^{11} s^{-1})	A_a (10^{11} s^{-1})	B^a	E (eV)	A_r (10^{11} s^{-1})	A_a (10^{11} s^{-1})	B^a
0.5	954.7	0.564	0.144	0.203	955.1	1.129	276.550	0.996
1.5	955.9	1.734	0.425	0.197	956.4	1.998	17.850	0.899
4.5	957.5	0.000	0.000	0.000	958.0	0.000	0.000	0.000
2.5	957.9	0.678	0.064	0.086	958.4	0.984	0.015	0.015
3.5	958.4	1.403	7.144	0.836	958.9	1.951	3.574	0.647
2.5	959.6	4.475	12.458	0.736	960.1	6.212	6.463	0.510
1.5	961.3	6.140	0.322	0.050	961.6	6.690	8.390	0.556
0.5	961.8	14.885	2.014	0.119	963.8	28.400	35.885	0.558
3.5	962.1	3.979	14.650	0.786	962.5	4.940	6.949	0.585
2.5	962.3	8.560	16.508	0.659	962.9	11.590	9.617	0.454
1.5	963.9	23.328	4.783	0.170	965.6	22.833	22.895	0.501
3.5	965.9	4.455	27.475	0.861	972.4	3.424	54.700	0.941
2.5	968.5	3.637	12.612	0.776	974.7	4.093	18.200	0.816
0.5	969.4	83.700	2.053	0.197	968.9	53.250	1148.000	0.956
1.5	970.9	88.475	21.540	0.196	973.2	47.850	690.250	0.935
1.5	976.5	7.183	0.578	0.075	976.9	6.952	102.325	0.936
2.5	977.1	2.502	6.930	0.735	977.5	2.957	2.557	0.464
2.5	978.2	8.708	0.445	0.049	978.7	14.785	0.033	0.002
3.5	978.7	6.878	21.350	0.756	979.2	8.625	8.146	0.486
1.5	981.7	74.050	18.478	0.200	984.4	202.775	346.750	0.631
2.5	984.7	5.067	21.605	0.810	991.1	5.832	45.467	0.886
0.5	987.6	366.600	91.650	0.200	988.6	369.450	0.354	0.001
1.5	989.8	281.750	68.200	0.195	995.3	151.975	408.000	0.729

[a]The levels listed are those that are predominantly $2p^5 3s 3d$; however, in some cases, the mixing is so large that the levels have nearly as much $2p^5 3p^2$ composition.

included the initial configurations $2p^6 3s + 2p^4 3s^2 3d + 2p^4 3s 3p^2 + 2p^4 3s 3d^2$ and the final configurations $2p^5 3s^2 + 2p^5 3s 3d + 2p^5 3p^2 + 2p^5 3d^2$. However, the ground-state level is very nearly pure $2p^6 3s$, and the mixing coefficients for the other configurations are so small that initial-state configuration interaction has a negligible effect on the cross section. On the other hand, the mixing between $2p^5 3s 3d$ and the other final-state configurations, especially $2p^5 3p^2$, is large. Nevertheless, since the collision strength from $2p^6 3s$ to $2p^5 3p^2$ and $2p^5 3d^2$ is zero, this final-state configuration interaction should have no effect on the total excitation cross section. This can be seen examining the upper portion of Fig. 2 where we compare the single-configuration and configuration-interaction calculations of this cross section. The $2p^6 3s \rightarrow 2p^5 3s^2$ transition with a threshold of about 868 eV has a nearly negligible cross section as compared to the $2p^6 3s \rightarrow 2p^5 3s 3d$ transition which has a threshold at about 955 eV. Configuration interaction has a noticeable effect on the excitation cross section to individual levels, in that it transfers collision strength from the levels of $2p^5 3s 3d$ to the levels of $2p^5 3p^2$; however, as expected, the total cross sections in the two calculations are identical.

The effect of configuration interaction on the branching ratios for autoionization is far from negligible. In a single-configuration approximation, the autoionizing rates from levels of $2p^5 3p^2$ and $2p^5 3d^2$ to $2p^6$ are much higher than those from levels of $2p^5 3s 3d$ to $2p^6$. Thus with configuration interaction included, the autoionizing rates from states that are still predominately $2p^5 3s 3d$ will increase by assuming some of the $2p^5 3p^2$ and $2p^5 3d^2$ character. Since the mixing between $2p^5 3s 3d$ and $2p^5 3p^2$ is by far the strongest, it is this interaction that will have the most pronounced effect on the autoionizing rates. The radiative rates will also be affected, since states from the $2p^5 3p^2$ configuration cannot radiate by a dipole transition and states of $2p^5 3d^2$ can only radiate to $2p^6 3d$, while states from $2p^5 3s 3d$ can radiate to both $2p^6 3s$ and $2p^6 3d$.

In Table I we show the excitation energies, radiative rates, autoionizing rates, and autoionizing branching ratios, with and without configuration interaction, for levels that have a predominant $2p^5 3s 3d$ character. Although the details are somewhat complicated by the fact that several levels are so highly mixed that it is difficult to associate them with a particular configuration, the overall effect is to increase the autoionizing rates, and thereby increase the branching ratios. The fact that the radiative rates for some of the levels increase with the inclusion of configuration interaction, rather than decrease as one might expect, is apparently due to variations of the intermediate-coupled eigenvectors within the $2p^5 3s 3d$ configuration when configuration interaction is included. However, the total radiative rate for all levels in Table I does decrease slightly.

In the bottom half of Fig. 2, we compare the $2p^63s \rightarrow 2p^53s^2$ and $2p^63s \rightarrow 2p^53s3d$ excitation-autoionization cross sections calculated with unit branching ratios, with configuration-interaction branching ratios, and with single-configuration branching ratios. At an energy of 1100 eV, the overall branching ratio is 0.27 with a single-configuration calculation, and 0.53 with configuration interaction. Thus, solely through its effect on the branching ratios, correlation is seen to increase the excitation-autoionization contributions associated with these particular inner-shell transitions by approximately a factor of 2.

Because of the negligible effect of configuration interaction in the initial state, all other excitation-autoionization transitions were calculated with a single-configuration $2p^63s$ initial level. Our results for the sum of all $2p^63s \rightarrow 2p^53snl$ ($n = 3,4,5$) transitions are shown in the top portion of Fig. 3. Again we compare the calculated cross sections with unit branching ratios, configuration-interaction branching ratios, and single-

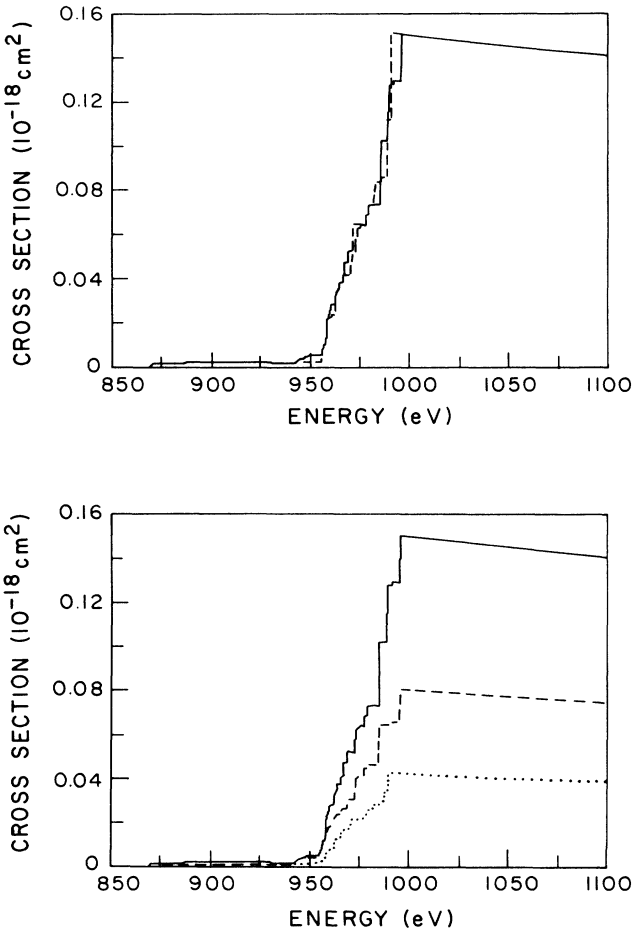

FIG. 2. Cross section for the $2p^63s \rightarrow 2p^53s^2$ and $2p^63s \rightarrow 2p^53s3d$ excitation-autoionization transition in Ni^{17+}. In the upper figure we employ a unit branching ratio for autoionization: dashed curve, single-configuration calculation; solid curve, configuration-interaction calculation. The bottom figure demonstrates the effects of configuration interaction on the autoionizing branching ratios: solid curve, configuration interaction and unit branching; dashed curve, configuration interaction with branching; dotted curve, single configuration with branching.

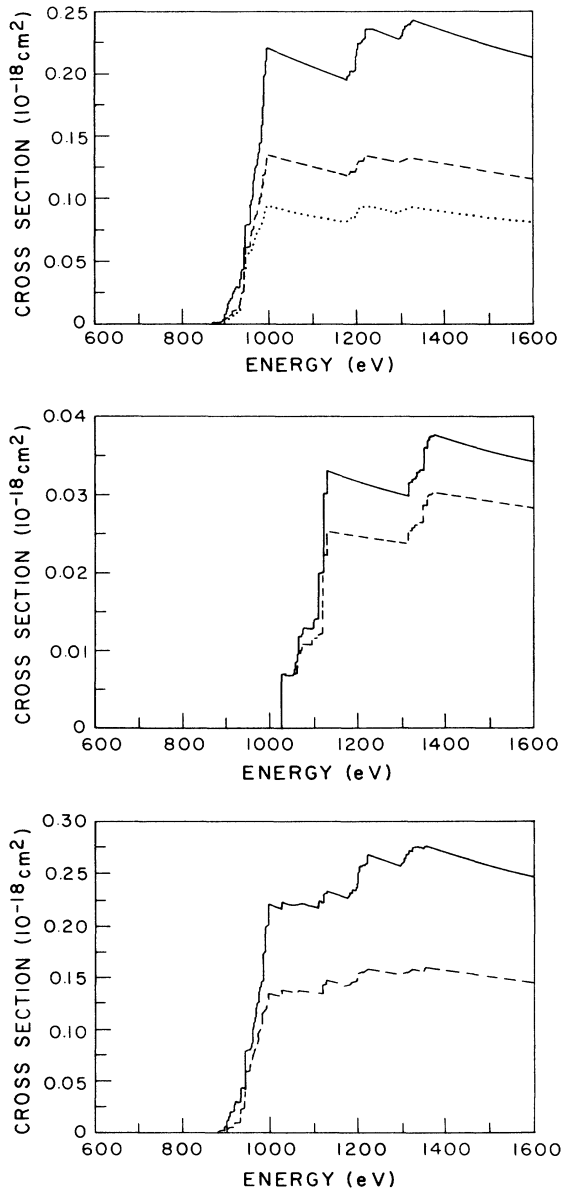

FIG. 3. Excitation-autoionization cross sections for Ni^{17+}. The top figure shows the cross section for the $2p^63s \rightarrow 2p^53snl$ transitions: solid curve, configuration interaction with unit branching; dashed curve, configuration interaction with branching; dotted curve, single configuration with branching. The middle figure shows the cross section for the $2p^63s \rightarrow 2s2p^63snl$ transitions: solid curve, configuration interaction with unit branching; dashed curve, configuration interaction with branching. The bottom figure shows the sum of the $2p^63s \rightarrow 2p^53snl$ and $2p^63s \rightarrow 2s2p^63snl$ cross sections: solid curve, configuration interaction with unit branching; dashed curve, configuration interaction with branching.

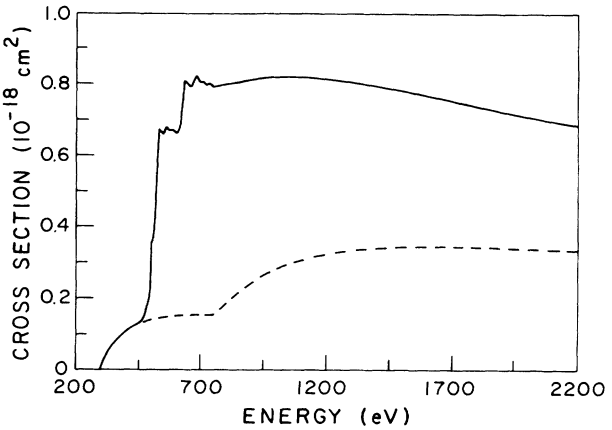

FIG. 4. Ionization cross section for Ti^{11+}. Solid curve, total-ionization cross section; dashed curve, direct-ionization contribution only.

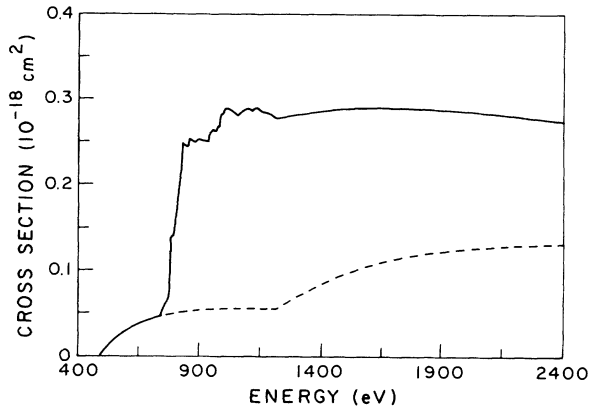

FIG. 6. Ionization cross section for Fe^{15+}. Same notation as in Fig. 4.

configuration branching ratios. The effects of configuration interaction are not as significant for the other transitions as they are for the $2p \rightarrow 3d$ transition. For example, for the $2p \rightarrow 3p$ transition, we included the interaction between $2p^5 3s 3p$ and $2p^5 3p 3d$. At 1100 eV the single-configuration branching ratios associated with this transition is 0.74, while with configuration interaction, this branching ratio is 0.77. As a result, at 1100 eV the overall branching ratios associated with the $2p \rightarrow 3l$ transitions, with and without configuration interaction, are 0.61 and 0.42, respectively. The overall configuration-interaction and single-configuration branching ratios associated with all $2p \rightarrow nl$ transitions at 1500 eV are 0.54 and 0.38, respectively.

In the case of the $2p^6 3s \rightarrow 2s 2p^6 3snl$ transitions, the single-configuration branching ratios are close to 1, since the states associated with the $2s 2p^6 3sns$ and $2s 2p^6 3snd$ configurations cannot make dipole transitions to bound states. However, with configuration interaction, such transitions are possible and the branching ratio is less than 1, as can be seen by examining the middle portion of Fig. 3. The overall branching ratio for the $2s \rightarrow nl$ transitions at an energy of 1500 eV is 0.86. Finally, in the bottom portion of Fig. 3, we compare the total excitation-autoionization cross section for the $2p \rightarrow nl$ and $2s \rightarrow nl$ transitions, with and without branching. The overall branching ratio for all excitation transitions at an energy of 1500 eV is 0.58.

B. Total-ionization cross sections and rate coefficients

The total-ionization cross sections for Ti^{11+}, Cr^{13+}, Fe^{15}, and Ni^{17+} are shown in Figs. 4 through 7, respectively. These calculations include direct ionization out of the $3s$, $2p$, and $2s$ subshells and the indirect excitation-autoionization transitions $2p^6 3s \rightarrow 2p^5 3s 3l$ ($l = 0,1,2$), $2p^6 3s \rightarrow 2p^5 3s 4l$ ($l = 1,2,3$), $2p^6 3s \rightarrow 2p^5 3s 5l$ ($l = 1,2,3$), $2p^6 3s \rightarrow 2s 2p^6 3s 3l$ ($l = 0,1,2$), and $2p^6 3s \rightarrow 2s 2p^6 3s 4l$ ($l = 0,1,2,3$). Transitions through the $2p^5 3s 4s$, $2p^5 3s 5s$, and $2p^5 3s 5g$ configurations were not included because of their extremely small cross sections. In Table II we give the direct-ionization threshold energies and the direct-ionization cross sections at twice

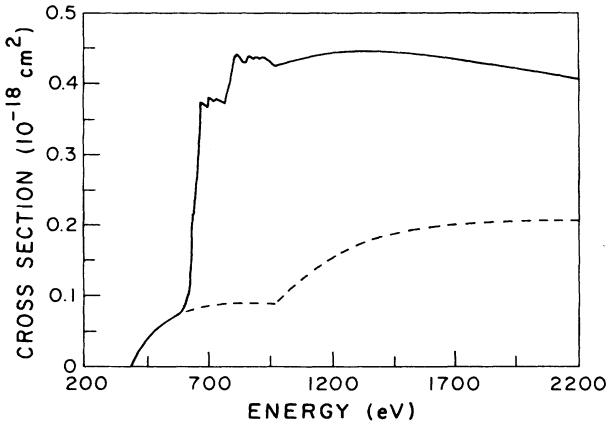

FIG. 5. Ionization cross section for Cr^{13+}. Same notation as in Fig. 4.

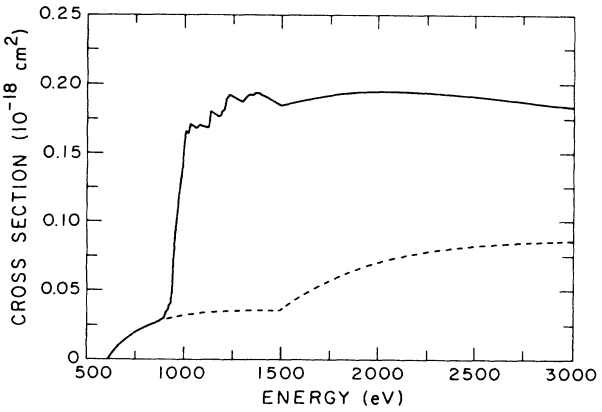

FIG. 7. Ionization cross section for Ni^{17+}. Same notation as in Fig. 4.

TABLE II. Direct-ionization thresholds and cross sections, at twice threshold, for the $3s$, $2p$, and $2s$ subshells.

	$3s$		$2p$		$2s$	
Ion	Threshold energy (eV)	σ (10^{-18} cm^2)	Threshold energy (eV)	σ (10^{-18} cm^2)	Threshold energy (eV)	σ (10^{-18} cm^2)
Ti^{11+}	291.8	0.150	752.5	0.189	856.1	0.038
Cr^{13+}	384.5	0.088	972.4	0.114	1089.9	0.023
Fe^{15+}	488.9	0.055	1219.0	0.073	1351.0	0.015
Ni^{17+}	607.5	0.035	1495.0	0.049	1643.0	0.010

threshold. In Table III we list the configuration-average threshold energies and cross sections for each of the indirect transitions.

We see by examining Figs. 4–7 that, as one would expect, the total cross sections decrease with ionization stage. The more abrupt change which occurs in going from Ti^{11+} to Cr^{13+} is due to the rather large decrease in the overall branching ratio for autoionization that occurs between these two ions. In Table IV we give the overall autoionization branching ratios at an energy approximately equal to 1.10 times the most energetic inner-shell excitation threshold, and the ratios of the total-ionization cross sections to the direct-ionization cross sections at the indirect cross-section peaks. We see from this table that the branching ratios decrease from 0.81 to 0.63 in going from Ti^{11+} to Cr^{13+}, but then only decrease slightly in going to the other two ions. The ratios of the total-ionization cross sections to the direct-ionization cross sections in the lower-energy region are reasonably close to 5 for all four ions.

In Fig. 8 we compare our calculated cross section with the crossed electron-ion beam measurements of the cross section[10] for Fe^{15+} in the energy region below 1000 eV. The data confirm the large contribution due to excitation autoionization, and are in reasonably good agreement with the calculations. Our calculated values are also in fairly good agreement with the configuration-average calculations of LaGattuta and Hahn[5] for the excitation-autoionization contributions. However, this appears to be fortuitous, since they only included the $2p \rightarrow 3l$ and $2s \rightarrow 3l$ transitions and used average branching ratios that are too small for the $2p^5 3s\,3d$ configuration and too large for the other configurations.

There is a good bit of scatter in the experimental data, and some of the data points are significantly higher than the calculated cross section. This may indicate the formation of recombination resonances of the form $2p^5 3snln'l'$ and $2s2p^6 3snln'l'$ in Fe^{14+} followed by sequential double autoionization to Fe^{16+} [see Eq. (3)], as first suggested by LaGattuta and Hahn.[5] However, the size of these resonances, if they do exist, are smaller than those predicted in Ref. 5, even though they used an electron-energy width in their calculation of 20 eV, which is at least a factor of 10 larger than the experimental width.

The source of the error in the calculation of resonant recombination followed by double autoionization in Ref. 5 may be the same configuration-interaction effects that we have found to be important in the calculation of autoionizing branching ratios for Fe^{15+}. The determina-

TABLE III. Configuration-average excitation energies and total cross sections, at threshold, for the inner-shell excitations $2p \rightarrow 3l, 4l, 5l$ and $2s \rightarrow 3l, 4l$.

	Ti^{11+}		Cr^{13+}		Fe^{15+}		Ni^{17+}	
Transition	ΔE (eV)	σ (10^{-18} cm^2)	ΔE (eV)	σ (10^{-18} cm^2)	ΔE (eV)	σ (10^{-18} cm^2)	ΔE (eV)	σ (10^{-18} cm^2)
$2p \rightarrow 3s$	453.2	0.008	579.2	0.005	720.5	0.003	876.9	0.002
$2p \rightarrow 3p$	476.3	0.263	606.5	0.168	752.0	0.112	913.0	0.077
$2p \rightarrow 3d$	513.4	0.422	649.5	0.290	801.0	0.206	968.1	0.150
$2p \rightarrow 4p$	598.1	0.051	780.1	0.032	972.2	0.021	1185.2	0.015
$2p \rightarrow 4d$	608.7	0.110	795.3	0.072	989.7	0.049	1205.1	0.034
$2p \rightarrow 4f$	627.9	0.012	803.0	0.008	999.0	0.006	1215.8	0.005
$2p \rightarrow 5p$	663.8	0.019	853.3	0.012	1065.9	0.008	1302.0	0.006
$2p \rightarrow 5d$	670.0	0.045	860.6	0.029	1074.4	0.019	1311.5	0.013
$2p \rightarrow 5f$	673.1	0.007	864.3	0.005	1078.8	0.004	1316.8	0.003
$2s \rightarrow 3s$	558.0	0.023	698.3	0.016	854.5	0.011	1026.9	0.008
$2s \rightarrow 3p$	580.2	0.016	724.5	0.011	884.8	0.008	1016.6	0.006
$2s \rightarrow 3d$	617.1	0.054	767.2	0.038	933.5	0.028	1116.4	0.020
$2s \rightarrow 4s$	702.0	0.008	885.5	0.005	1090.3	0.003	1316.9	0.002
$2s \rightarrow 4p$	712.4	0.004	897.8	0.003	1104.7	0.002	1333.4	0.001
$2s \rightarrow 4d$	725.3	0.013	912.9	0.009	1122.1	0.006	1353.1	0.004
$2s \rightarrow 4f$	731.5	0.003	920.5	0.002	1131.2	0.001	1377.3	0.001

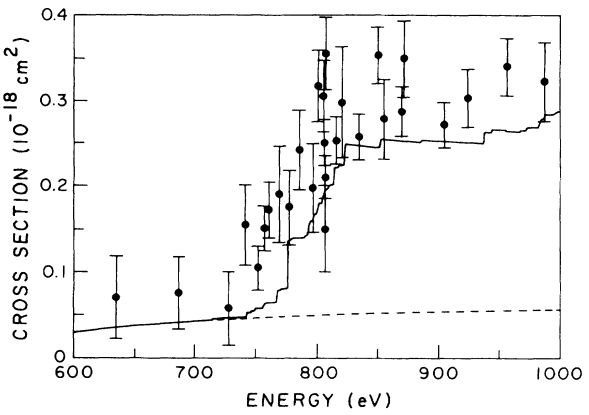

FIG. 8. Ionization cross section for Fe^{15+} in the near-threshold region for excitation autoionization. Same notation as in Fig. 4. The experimental points are from Ref. 10.

tion of resonance contributions to the ionization cross section of Fe^{15+} involves complex calculations of the branching ratios for autoionization from Fe^{14+} to the autoionizing levels of Fe^{15+} versus autoionization to bound levels of Fe^{15+} and radiation to bound levels of Fe^{14+}, as well as the branching ratios for autoionization from Fe^{15+} to Fe^{16+} versus radiation to bound levels of Fe^{15+}. To simplify the calculation, LaGattuta and Hahn[5] employed average branching ratios for autoionizing and radiative transitions between configurations, rather than individual branching ratios for transitions between levels. This in itself can lead to significant errors, but when configuration interaction is important, these errors can be particularly sizeable. However, to determine the proper branching ratios for transitions between individual levels, with the inclusion of correlation, would require a very large calculation because of the number of levels involved.

The results of our calculations of the ionization rate coefficients for all four ions are presented in Figs. 9 through 12. In addition, the natural logarithms of the rate coefficients have been fitted to the Chebyshev polynomial expansion [Eqs. (21)–(22)], and the fitting coefficients and values of $E_{\min}$ and $E_{\max}$ are listed in Table V. By examining the figures, we see that the excitation-autoionization contributions about double the rates near the maxima, and have an even larger effect at lower temperatures. In the last two columns of Table IV we give the ratios of the total rate coefficients to the direct-ionization rate coefficients at temperatures of 500 and 2000 eV. Our ratio of 3.0 for Fe^{15+} at a temperature of 500 eV compares to the value of approximately 2.5 determined by Cowan and Mann.[4] Our higher value is due to both the fact that our overall branching ratio for autoionization is higher than theirs, and Seaton's semiempirical formula for the direct-ionization rate coefficient, which they employed, is higher than our distorted-wave direct-ionization rate coefficient.

IV. CONCLUSIONS

We have calculated the ionization cross sections and rate coefficients for the Na-like ions Ti^{11+}, Cr^{13+}, Fe^{15+}, and Ni^{17+} over a wide range of energies and temperatures. The contributions of excitation autoionization to the cross sections and rates are found to be large in all four ions, even though radiative relaxation substantially reduced the indirect contribution, especially for the last three species. Initial-state configuration interaction has a negligible effect on the inner-shell excitation cross sections, and final-state configuration interaction has a negligible effect on the total inner-shell excitation cross section but a pronounced effect on the autoionizing branching ratios.

The small effect of configuration interaction on $\Delta n \geq 1$ excitations in highly ionized species may be quite general, and not just restricted to Na-like ions. The reason for this is that configuration interaction in highly ionized atoms is only important between configurations within a complex. So that, for example, if we consider $\Delta n = 1$ excitations such as $3p^6 \rightarrow 3p^5 4d$ in Ar-like ions, the most important initial-state configuration interaction occurs between $3p^6$ and $3p^4 3d^2$; however, the collision strength for the transition $3p^4 3d^2 \rightarrow 3p^5 4d$ is zero and the effect of this interaction on the cross section is small. The same would be true of the important final-state interac-

TABLE IV. Overall autoionizing branching ratios, ratios of total-ionization cross sections to direct-ionization cross sections, and ratios of total-ionization rate coefficients to direct-ionization rate coefficients.

Ion	Branching ratios E (eV)[a]	B[a]	Ratios of total- to direct-ionization cross sections E (eV)[b]	σ_T/σ_D	Ratios of total- to direct-ionization rate coefficients α_T/α_D ($kT=500$ eV)	α_T/α_D ($kT=2000$ eV)
Ti^{11+}	800.0	0.81	680.0	5.4	2.8	2.1
Cr^{13+}	1000.0	0.63	875.0	4.9	2.7	2.0
Fe^{15+}	1250.0	0.60	1100.0	5.3	3.0	2.1
Ni^{17+}	1500.0	0.58	1370.0	5.4	3.3	2.3

[a]Energies at which the overall branching ratios were calculated; they are approximately equal to 1.10 times the threshold energy of the most energetic inner-shell excitation.

[b]Energies at which the ratios were calculated; they are the energies at which the indirect contributions are at a maximum.

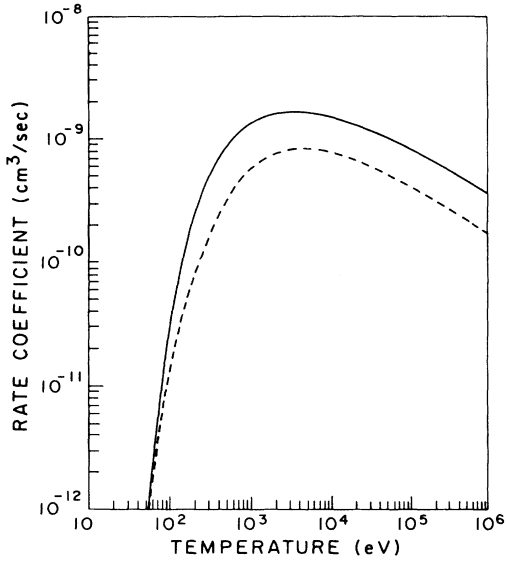

FIG. 9. Ionization rate coefficient for Ti^{11+}. Solid curve, total rate coefficient; dashed curve, direct contribution only.

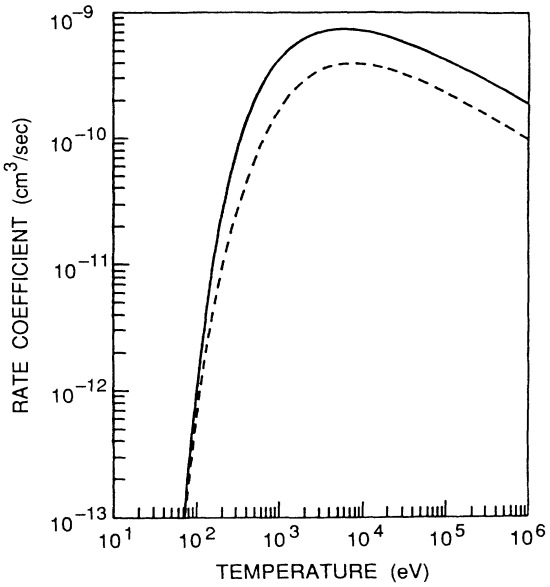

FIG. 11. Ionization rate coefficient for Fe^{15+}. Same notation as in Fig. 9.

tions. This is, of course, not true for $\Delta n = 0$ excitations such as $3p^6 \rightarrow 3p^5 3d$, since the collision strength for $3p^4 3d^2 \rightarrow 3p^5 3d$ is comparable in magnitude to that of the primary transition. However, since $\Delta n = 0$ excitations do not in general end up in autoionizing states in highly ionized species, it may be true that the inner-shell excitations which contribute to electron-impact ionization in such ions can be calculated with reasonably good accuracy using a single-configuration approximation. However, as we have seen, once radiative decay to bound states becomes comparable to autoionization, configuration interaction in the final state must be included in order to obtain accurate branching ratios for autoionization.

One effect which could influence these results is possible interference between autoionization and radiative relaxation. Armstrong *et al.*[21] have shown that if the radiative rates are comparable to the autoionizing rates and there is strong radiation field coupling between the final states resulting from autoionization with the final states resulting from radiative relaxation, the branching ratio for autoionization can be significantly affected. For

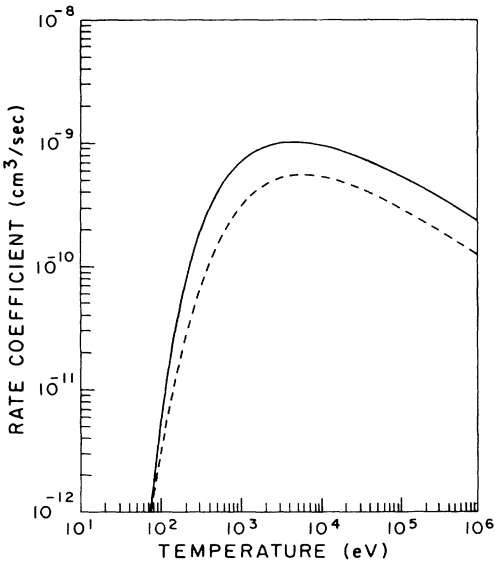

FIG. 10. Ionization rate coefficient for Cr^{13+}. Same notation as in Fig. 9.

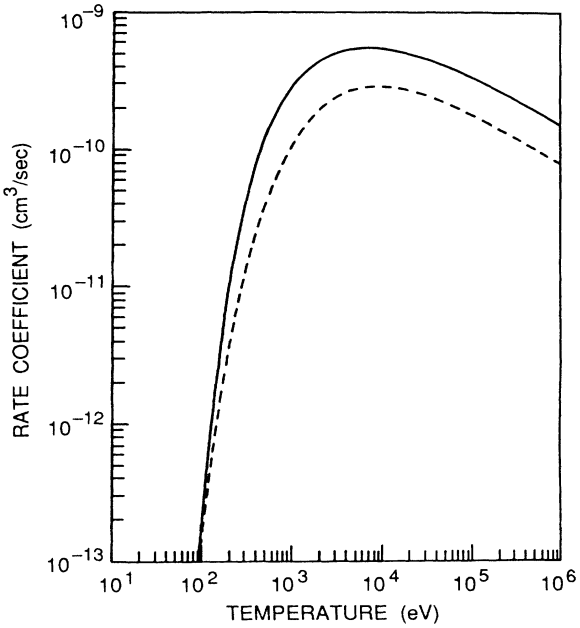

FIG. 12. Ionization rate coefficient for Ni^{17+}. Same notation as in Fig. 9.

TABLE V. Rate coefficient fitting parameters. E_{min} and E_{max} are the minimum and maximum values of kT over which the fit is valid, and are used to calculate the variable x from Eq. (22). The fitting parameters, a_0 through a_8, can be used in Eq. (21) to calculate the rate coefficient in units of cm^3/s.

	Ti^{11+}	Cr^{13+}	Fe^{15+}	Ni^{17+}
E_{min} (eV)	5.3×10^1	7.3×10^1	7.0×10^1	9.1×10^1
E_{max} (eV)	1.0×10^6	1.0×10^6	1.0×10^6	1.0×10^6
a_0	−44.059 900 0	−44.822 310 0	−46.164 790 0	−46.589 240 0
a_1	1.741 925 0	1.641 249 0	2.357 747 0	2.284 531 0
a_2	−2.172 249 0	−2.038 063 0	−2.505 344 0	−2.393 890 0
a_3	1.030 038 0	0.953 929 5	1.202 328 0	1.141 181 0
a_4	−0.442 797 0	−0.399 494 0	−0.511 093 0	−0.486 273 5
a_5	0.159 279 6	0.151 139 4	0.189 448 4	0.184 636 2
a_6	−0.051 754 7	−0.046 806 2	−0.053 514 8	−0.056 565 2
a_7	0.004 930 6	0.009 403 8	0.006 009 3	0.010 650 4
a_8	0.000 901 6	0.002 516 8	0.006 868 8	0.002 926 3

the simple case of one autoionizing state and one bound state of the N-electron ion, and one state of the $(N-1)$-electron ion plus free electron, it is shown in Ref. 21 that the branching ratio for autoionization, B^a, is approximately

$$B^a=\left[\frac{B_0^a}{(1+A_r/q^2A_a)}\right]\left[1+\frac{A_r^2}{q^2A_a^2}\right], \tag{23}$$

where B_0^a is the branching ratio with no interference [see Eq. (5)] and q is the Fano q parameter.[22] This correction to the branching ratio for autoionization corresponds physically to the free electron emitted in the autoionizing event undergoing recombination to the final bound state. Obviously, in the weak coupling limit when q is large, B^a reduces to B_0^a.

Although for many of the states included in these calculations the radiative and autoionizing rates are comparable, we expect that in most cases the q values will be quite large. We have not made any explicit calculations for radiative decay to the $2p$ subshell in these ions to support this premise. However, we have carried out such calculations for radiative transitions into the $2s$ subshell in Fe^{23+} and the $3s$ subshell in Fe^{15+} while investigating possible interference effects between dielectronic and radiative recombination.[23] In these cases the values of q^2 were found to be of order 10^3 to 10^4. Furthermore, Jacobs *et al.*[24] have computed q values for radiative transitions into the $1s$ subshell in Ar^{15+} and Ar^{16+} and found that the q values for most transitions are quite large. On this basis, we believe that such interference effects should be negligible for nearly all the transitions involved here.

Another effect that could influence the accuracy of these calculations is coupling between scattering channels. As mentioned in Sec. I, coupling effects are, in general, expected to be relatively small in highly ionized systems. It is obvious that coupling between channels associated with the initial and final levels will be negligible in such ions. However, it is not clear that the coupling between the channels corresponding to nearby levels within a configuration, or closely spaced levels within a complex of configurations, can be neglected, even in high stages of ionization. A systematic study comparing the distorted-wave approximation with the close-coupling approximation (with the same set of bound-state wave functions) as a function of ionization stage is needed to investigate this possibility. Of course, because of the importance of the spin-orbit interaction and other relativistic effects in highly ionized atoms, this would require the use of a close-coupling code in which coupling is considered between scattering channels formed from intermediate-coupled levels rather than LS terms.

Finally, it is not clear from our comparison of the experimental and theoretical cross sections for Fe^{15+} whether resonance recombination followed by double autoionization contributes to indirect ionization. An experiment is currently being planned by Gregory and Phaneuf at Oak Ridge National Laboratory[25] to measure the cross section of Ti^{11+}. For this lower stage of ionization, the ion current from their electron-cyclotron-resonance (ECR) source will be higher than in the case of Fe^{15+}, and it should be possible to measure the cross section with greater accuracy in the region where recombination resonances may occur. It will be interesting to see whether a comparison of these new measurements with our calculated cross sections will reveal, with some reliability, the presence of these resonances.

ACKNOWLEDGMENTS

We wish to thank R. D. Cowan for making his atomic structure programs available to us, and for a number of useful discussions. We would also like to thank D. C. Gregory and R. A. Phaneuf for discussions regarding the cross-section measurements of Fe^{15+} and the experiment being planned with Ti^{11+}, and H. T. Hunter and D. C. Gregory for performing the fits of the ionization rate coefficients. One of us (D.C.G.) would like to thank the Joint Institute for Laboratory Astrophysics for their hospitality and financial support through the JILA Visiting Fellow Program. This work was partially supported by the Office of Fusion Energy, U.S. Department of Energy, under Contract No. DE-AC05-840R21400 with Martin Marietta Energy Systems, Inc. and Contract No. DE-FG05-86ER53217 with Auburn University.

*Permanent address: Department of Physics, Rollins College, Winter Park, FL 32789.
†Permanent address: Physics Division, Oak Ridge National Laboratory, Oak Ridge, TN 37831.

[1]O. Bely, Ann. Astrophys. **30**, 953 (1967).
[2]O. Bely, J. Phys. B **1**, 23 (1968).
[3]D. L. Moores and H. Nussbaumer, J. Phys. B **3**, 161 (1970).
[4]R. D. Cowan and J. B. Mann, Astrophys. J. **232**, 940 (1979).
[5]K. J. LaGattuta and Y. Hahn, Phys. Rev. A **24**, 2273 (1981).
[6]S. O. Martin, B. Peart, and K. T. Dolder, J. Phys. B **1**, 537 (1968).
[7]D. H. Crandall, R. A. Phaneuf, R. A. Falk, and G. H. Dunn, Phys. Rev. A **25**, 143 (1982).
[8]D. C. Griffin, C. Bottcher, and M. S. Pindzola, Phys. Rev. A **25**, 154 (1982).
[9]R. J. W. Henry and A. Z. Msezane, Phys. Rev. A **26**, 2545 (1982).
[10]D. C. Gregory, L. J. Wang, K. Rinn, and F. W. Meyer, Phys. Rev. A **35**, 3256 (1987).
[11]R. K. Peterkop, Zh. Eksp. Teor. Fiz. **41**, 1938 (1961) [Sov. Phys.—JETP **14**, 1377 (1962)].
[12]R. D. Cowan and D. C. Griffin, J. Opt. Soc. Am. **66**, 1010 (1976).
[13]M. E. Riley and D. G. Truhlar, J. Chem. Phys. **63**, 2182 (1975).
[14]S. M. Younger, Phys. Rev. A **24**, 1272 (1981).
[15]R. D. Cowan, *The Theory of Atomic Structure and Spectra* (California Press, Berkeley, 1981).
[16]M. S. Pindzola, D. C. Griffin, and C. Bottcher, Phys. Rev. A **33**, 3787 (1986).
[17]M. G. Cox and J. G. Hayes, U.K. National Physical Laboratory Report No. NAC 26, 1973 (unpublished).
[18]See, for example, *Handbook of Mathematical Functions,* edited by Milton Abramowitz and Irene A. Stegun (Dover, New York, 1970), p. 795.
[19]C. W. Clenshaw, Math. Tables Comp. **9**, 118 (1955).
[20]M. S. Pindzola, D. C. Griffin, C. Bottcher, S. M. Younger, and H. T. Hunter, Oak Ridge National Laboratory Report No. ORNL/TM-10297, 1987 (unpublished).
[21]Lloyd Armstrong, Jr., Constantine E. Theodosiou, and M. J. Wall, Phys. Rev. A **18**, 2538 (1978).
[22]U. Fano, Phys. Rev. **124**, 1866 (1961).
[23]D. C. Griffin and M. S. Pindzola, Phys. Rev. A **35**, 2821 (1987).
[24]V. L. Jacobs, J. E. Rogerson, M. H. Chen, and R. D. Cowan, Phys. Rev. A **32**, 3382 (1985).
[25]D. C. Gregory and R. A. Planeuf (private communication).